

# The Hydration Structure of the Elusive Ac(III) Aqua Ion: Interpretation of XAS Spectra on the Basis of MD Simulations.

Rafael R. Pappalardo, Daniel Z. Caralampio, José M. Martínez, and Enrique  
Sánchez Marcos\*

*Departamento de Química Física, Universidad de Sevilla, 41012 Sevilla, Spain*

E-mail: [sanchez@us.es](mailto:sanchez@us.es)

Phone: +34 955421005

## Abstract

Actinoid solution chemistry knowledge has been enriched with the recent synthesis and characterization of the elusive Ac(III) aqua ion, the first one of the series, for which EXAFS and XANES spectra has been recorded. Structural analysis combined with Born-Oppenheimer molecular dynamics simulations lead to suggest a 2.63-2.69 Å range for the Ac-O distance, and a coordination number between 9 and 11. A hydration number as high as 11 would imply the appearance of a sharp coordination number contraction at the beginning of the series. In this work we present a specific Ac(III)-H<sub>2</sub>O first-principles based intermolecular potential which has been developed following the exchangeable Hydrated Ion model. This potential has been used in classical Molecular Dynamics simulations of Ac(III) in water. Results show a well-defined Ac(III) enneahydrated aqua ion with a mean Ac-O distance of  $2.66 \pm 0.02$  Å, surrounded by a compact second hydration shell formed by  $\sim 20$  H<sub>2</sub>O centered

at  $4.9 \pm 0.1 \text{ \AA}$ . The results obtained for the first element of the actinoid series confirm the regular contraction of their aqua ions along the series. Simulated EXAFS and XANES spectra have been computed from the structural information provided by the MD simulation. The agreement with the experimental spectra is satisfactory validating the computer simulation results. An observed hump in the experimental XANES spectrum is interpreted and ascribed to the second hydration shell, being an evidence of the consistency of the Ac(III) hydration shells.

## Introduction

Actinoid solution chemistry is a crucial topic involving many fields of Chemistry, Physics, Chemical Engineering, Medicine, Pharmacology and Environmental Science.<sup>1,2</sup> The knowledge of the physicochemical properties of actinoid ions in solution is important in determining strategies to manage and recycle nuclear fuel, in mitigating environmental problems derived from natural waters contamination or in deeping insight into the understanding of the pharmacological behavior in radiotherapy for treating cancer through a new process called targeted alpha-particle therapy.<sup>3-6</sup>

Whereas the chemical behavior of lanthanoids, the first f-transition series, is well-known, this is not the case for most actinoids. This is due to the experimental difficulties derived from the limited availability of many of these elements, the high radioactivity of most of their samples, as well as the chemical instability of their ions and compounds. This is the case of the first element of the series, the Actinium, whose trivalent oxidation state,  $\text{Ac}^{3+}$ , aqueous solution has only been synthesized very recently and characterized by the EXAFS and XANES spectra recorded by Ferrier et al.<sup>7</sup> They established a sophisticated and improved procedure<sup>8</sup> to obtain micrograms of the actinoid cation, an amount that allows an  $\text{Ac}^{3+}$  aqueous solution concentrated enough to record its XAS spectra. The structural results derived from the EXAFS fitting provide a hydration number for the aqua ion of  $10.9 \pm 0.5$  at an average Ac-O distance of  $2.63 \pm 0.01 \text{ \AA}$ . The Debye-Waller factor

(DW) was fixed during the experimental fitting to  $0.009 \text{ \AA}^2$ , a value extrapolated from a linear correlation based on the values published for the U-Cf aqua ions series. Ferrier et al.<sup>7</sup> also carried out Born-Oppenheimer MD simulations, using the PBE DFT functional, of one  $\text{Ac}^{3+}$  cation plus 64  $\text{H}_2\text{O}$  to provide additional XAS-independent information. This simulation predicted an aqua ion with nine instead of eleven water molecules in the first shell and a mean Ac-O distance of  $2.69 \pm 0.11 \text{ \AA}$ . In a previous work, the same group<sup>8</sup> reported the first Ac- $\text{O}_{\text{H}_2\text{O}}$  distance,  $2.59 \text{ \AA}$ , from the fitting of the experimental EXAFS spectrum of a concentrated HCl aqueous solution containing  $\text{Ac}^{3+}$ , where its most probable first coordination was  $\text{Ac}(\text{H}_2\text{O})_{6.6}\text{Cl}_{3.2}$ . In a very recent work,<sup>9</sup> they have just determined the structure of the  $\text{Ac}^{3+}$  aqua ion in nitrate solutions by means of EXAFS, proposing the same Ac-O distance and a coordination number of  $10 \pm 1$ . This set of results leads to a range of coordination numbers for the aqua ion between 9 and 11, and an Ac- $\text{O}_{\text{H}_2\text{O}}$  distance in the range of  $2.59\text{--}2.69 \text{ \AA}$ . When dealing with a challenging chemical problem such as the  $\text{Ac}^{3+}$  solution chemistry, the uncertainties in the experimental and theoretically predicted values are larger than in those cases where the methods and the experimental availability are conventional. Due to the position of Ac at the beginning of the series, the possibility of a coordination number as high as 11 opens the door to reexamine if the proposed actinoid aqua ion contraction in solution exhibits a similar behavior to that observed in the lanthanoid case.<sup>10-13</sup> In addition, the ion size evolution through the series is also interesting. This is a key property in relating the physicochemical properties of a given stable and safe lanthanoid ion to an hazardous and unstable actinoid ion.<sup>14</sup>

The aim of this theoretical work is to provide additional and independent information on the  $\text{Ac}^{3+}$  hydration by means of classical Molecular Dynamics based on the construction of a specific  $\text{Ac}^{3+}\text{--H}_2\text{O}$  intermolecular potential using a refined extension of our statistical implementation of the Hydrated Ion model.<sup>15</sup> This extension has already been successfully applied to solve the hydration structure of other highly-charged metal aqua ions that exchange water molecules in their first hydration shell during the simulation time.<sup>16-18</sup> In fact, before the appearance of the experimental  $\text{Ac}^{3+}$  aqua ion structure determined by

Ferrier et al., we carried out a preliminar classical MD simulation of  $\text{Ac}^{3+}$  in water within a general study on the aqua ion coordination geometry of some lanthanoid and actinoid aqua ions.<sup>19</sup> An ennea-hydrate with an  $\text{Ac}-\text{O}_{\text{H}_2\text{O}}$  distance of 2.65 Å was obtained. In previous studies,<sup>16,20-22</sup> we had also combined the MD structural information of several aqueous solutions containing highly-charged d- and f-transition metal ions with the ab initio full-multiple scattering formalism developed by Rehr et al.<sup>23,24</sup> and implemented in the FEFF program,<sup>25</sup> obtaining successful comparisons with experimental spectra.

## Computational Methods

The  $\text{Ac}^{3+}-\text{H}_2\text{O}$  and  $\text{H}_2\text{O}-\text{H}_2\text{O}$  intermolecular potentials are built on the basis of the flexible and polarizable MCDHO model.<sup>26</sup> In this work, the MCDHO2 version has been used because it provides a better water mobility.<sup>27</sup> The basic idea of the Hydrated Ion model is to extract an average ab initio pair interaction,  $\text{M}^{\text{P}^+}-\text{H}_2\text{O}$  from the quantum-mechanical information of the hydrated ion  $[\text{M}(\text{H}_2\text{O})_m]^{\text{P}^+}$ , being  $m=9$  and  $10$  for the  $\text{Ac}^{3+}$  case, when different arrangements of water molecules are considered. Figure S1 of the Supporting Information (SI) collects representative structures computed quantum-mechanically to build the interaction potential. A total of 325 structures were used. The QM interaction energy is fitted to a functional form depending on structural parameters. Details of the general procedure can be found in previous works.<sup>17,19</sup> Text and Figure S2 in SI provide the functional form of the potential and details on the QM computations, which were carried out at the DFT level using the TPSSh<sup>28</sup> functional. Gaussian 09 program<sup>29</sup> was used for the QM calculations. In Tables S1 and S2 of SI the parameters of the developed  $\text{Ac}^{3+}-\text{H}_2\text{O}$  potential as well as those of the MCDHO2<sup>27</sup> for the water model can be found. Figure S3 in SI shows the goodness of the ion-water potential fit by plotting the interaction potential energy vs. the QM energy for the structures employed in the potential building. The standard deviation of the fit was 2.4 kcal/mol.

Classical NVT MD simulations of a system formed by one  $\text{Ac}^{3+}$  and 1000  $\text{H}_2\text{O}$  were

carried out at 300 K. A modified version of the DL-POLY classic code<sup>30</sup> was used for the MD simulations. Box length was fixed to reproduce the experimental water density at 1 atm. Initial structure was taken from an already thermalized box.<sup>19</sup> After a thermalization period of 100 ps, 10 ns were produced to perform the analysis, employing a timestep of 0.1 fs.

## Results and Discussion

Table 1: Interaction energies (kcal/mol) for several  $\text{Ac}^{3+}$  hydrates.

Structure	$E_{\text{int}}$ (kcal/mol)		
	QM//QM	Pot//QM	Pot//Pot
$[\text{Ac}(\text{H}_2\text{O})_8]^{3+}$	-413.9	-416.1	-417.4
$[\text{Ac}(\text{H}_2\text{O})_8]^{3+}(\text{H}_2\text{O})_1$	-442.6	-442.1	-443.8
$[\text{Ac}(\text{H}_2\text{O})_9]^{3+}$	-438.1	-438.1	-439.3
$[\text{Ac}(\text{H}_2\text{O})_9]^{3+}(\text{H}_2\text{O})_1$	-463.3	-461.1	-463.0
$[\text{Ac}(\text{H}_2\text{O})_{10}]^{3+}$	-454.5	-452.6	(a)
$[\text{Ac}(\text{H}_2\text{O})_8]^{3+}(\text{H}_2\text{O})_{16}$	-727.9	-720.9	-724.1
$[\text{Ac}(\text{H}_2\text{O})_9]^{3+}(\text{H}_2\text{O})_{18}$	-748.5	-742.8	-750.5

(a) optimized structure is (9,1).

Table 1 shows the performance of the potential for the most representative  $\text{Ac}^{3+}$  clusters,  $[\text{Ac}(\text{H}_2\text{O})_m]^{3+}(\text{H}_2\text{O})_n$ , Column QM//QM collects the interaction energy,  $E_{\text{int}}$ , for optimized clusters with one shell ( $m=8, 9$  or  $10$ ), two shells ( $n=16,18$ ) or only one water molecule in the second shell, which forms a double hydrogen bond with two first-shell water molecules due to the lack of more second-shell water molecules. Pot//QM and Pot//Pot collect the  $E_{\text{int}}$  values obtained with the developed potential at the QM or potential optimized geometries, respectively. The agreement is satisfactory for the octa- and ennea-hydrate, as well as for their two-shell aggregates. It is remarkable how for the two-shell  $[\text{Ac}(\text{H}_2\text{O})_m]^{3+}(\text{H}_2\text{O})_n$  clusters, the energy gap between the QM and the potential at the same geometry is less than 1%. It is worth pointing out that these clusters represent much larger structures than those used in the fitting and represent realistic

arrangements in solution. For instance, for  $m=9$  and  $n=18$ ,  $E_{\text{int}}^{\text{QM}/\text{QM}} = -748.5$  kcal/mol vs.  $E_{\text{int}}^{\text{Pot}/\text{QM}} = -742.8$  kcal/mol or  $E_{\text{int}}^{\text{Pot}/\text{Pot}} = -750.5$  kcal/mol. These results verify the appropriate performance of the potential when a complete second hydration shell is present. Moreover, it is also interesting to point out that optimized structures using the classical potential are very close to the QM ones, both at energetical and structural levels (see  $R_{\text{M-O}}$  columns in Table S4 of SI). The main difference is found for the deca-hydrated structure. Optimized QM computations (QM//QM) find a minimum geometry where ten  $\text{H}_2\text{O}$  are in the first shell whereas the potential (Pot//Pot) predicts a (9,1) structure. In fact, the geometrical optimization of the decahydrate with the classical potential leads to the same optimized structure obtained for the (9,1) when the potential is employed. In addition, this (9,1) structure has almost the same geometry as that obtained by the QM computations. That is, there is a QM (9,1) geometry that corresponds to a minimum having a lower energy than that of the decahydrate. This shows that both levels, QM and classical potential, support the prevalence of the ennea-hydration in gas phase clusters. Any case, this is a minor issue as we are interested in the description of the liquid state where the representative arrangements are defined by complete hydration shells.

The preference for the ennea-coordination in the first shell is also supported by the  $E_{\text{int}}$  comparison for different arrangements. Let us consider  $\text{Ac}^{3+}$  clusters bearing nine water molecules, (8,1) or (9,0), or ten water molecules: (8,2), (9,1) or (10,0), where second-shell water molecules are forming one single hydrogen bond with those of the first shell, as happens in solution. To compute  $E_{\text{int}}$  all second-shell water molecules but two or one, as can be seen in Figure S4 of SI, were removed from the two complete shell structures, (8,16) and (9,18), respectively. The interaction energy between a water molecule in the second shell and the aqua ion,  $\Delta E^{\text{QM}}$ , is computed as

$$\Delta E^{\text{QM}} = E^{\text{QM}}([\text{Ac}(\text{H}_2\text{O})_m]^{3+} \cdot \text{H}_2\text{O}) - E^{\text{QM}}([\text{Ac}(\text{H}_2\text{O})_m]^{3+}) - E^{\text{QM}}(\text{H}_2\text{O}) \quad (1)$$

$\Delta E^{\text{QM}}$  values are -18.7 kcal/mol for  $m = 8$  and -18.5 kcal/mol for  $m = 9$ . Thus, the total

$E_{\text{int}}^{\text{QM}}$  of the  $\text{Ac}^{3+}$  octahydrate bearing two second-shell water molecules involved in single hydrogen bonds is computed as

$$E_{\text{int}}^{\text{QM}}([\text{Ac}(\text{H}_2\text{O})_8]^{3+}) + 2\Delta E^{\text{QM}}(m = 8) = -451.3\text{kcal/mol}. \quad (2)$$

In the case of the  $\text{Ac}^{3+}$  enneahydrate and one second-shell water molecule that forms a single hydrogen bond, the expression applied is similar and the value becomes  $-456.6$  kcal/mol. This leads to the following  $E_{\text{int}}^{\text{QM}}$  order for the 10-water molecules  $\text{Ac}^{3+}$  clusters:  $-456.6(9, 1) < -454.5(10) < -451.3(8, 2)$  kcal/mol. In the case of 9-water molecules, the value for (9,0) is  $-438.1$  kcal/mol, smaller than for (8,1),  $-432.6$  kcal/mol. Similar conclusion is reached if  $E_{\text{int}}^{\text{Pot}}$  values derived from the potential developed are examined.

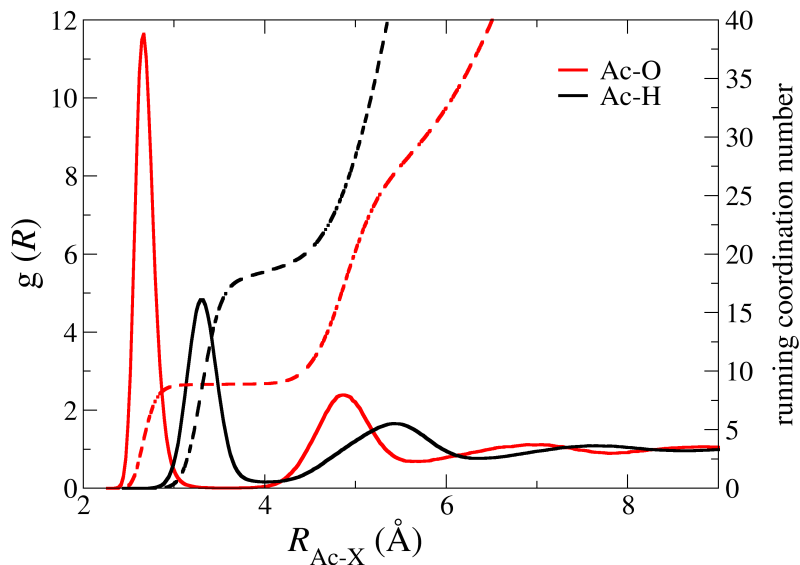


Figure 1: Ac-O and Ac-H RDFs (solid lines) and their corresponding running integration numbers (dashed lines).

Ac-O and Ac-H radial distribution functions (RDF) are shown in Figure 1. There are sharp first peaks centered at  $2.66 \pm 0.02 \text{ \AA}$  and  $3.30 \pm 0.03 \text{ \AA}$  for the Ac-O and Ac-H distances, respectively. The corresponding coordination numbers are 8.9 and  $\sim 19$ . Ferrier et al. have obtained from EXAFS fitting of two samples containing the  $\text{Ac}^{3+}$  aqua

ion an Ac-O distance of  $2.63\pm 0.01$  Å and a coordination number of  $10.9\pm 0.5$  in triflic acid solution,<sup>7</sup> and  $10\pm 0.9$  in dilute nitric acid solution.<sup>9</sup> A depletion zone separates the first from the second hydration shell. This indicates the existence of a robust  $\text{Ac}^{3+}$  enneahydrated aquaion. This structural consistency joined to its high charge determine a well defined second hydration shell formed by  $\sim 20$  water molecules where the Ac-O distance is centered at  $4.9\pm 0.1$  Å. Table 2 collects a set of  $\text{Ac}^{3+}$  aqueous solution properties. The mean residence time (MRT) of the first-shell water molecules has been computed by means of the Impey et al. method<sup>31</sup> using two criteria for the parameter  $t^*$ , i.e. the allowed time for a water molecule to leave the first shell without losing its adscription to it. The MRT values obtained are  $410\pm 10$  ps ( $t^*=0$  ps) and  $623\pm 15$  ps ( $t^*=2$  ps). These values confirm the  $[\text{Ac}(\text{H}_2\text{O})_9]^{3+}$  consistency and justifies the depletion zone observed in the RDFs. This idea is reinforced by the strong polarization of the first-shell water molecules which increase their dipole moment by 0.6 D ( $\Delta\mu_{\text{I}}$ ) with respect to the bulk value. The polarization is extended even to the second shell ( $\Delta\mu_{\text{II}} = 0.1$  D). The tilt angle formed by the Ac-O<sub>I</sub> vector and the water molecule plane gives an useful information on the perturbation imposed by the monoatomic cation on its first hydration shell. A tilt angle value of  $0^\circ$  (perfect cation-dipole orientation) indicates that the cation is contained in the water molecule plane and that a strong interaction is present. Contrarily, the absence of intermolecular interaction corresponds to an uncorrelated tilt angle. For the first shell, the tilt angle is close to  $30^\circ$  whereas it increases up to  $\sim 60^\circ$  for the second shell. Apart from the consistency of the  $\text{Ac}^{3+}$  aqua ion, two additional parameters can provide additional structural information to characterize it. One of these parameters is the molecular eccentricity<sup>32</sup> that is calculated as the distance between the metal cation position and the mass center of the first hydration shell. A symmetric arrangement would have a molecular eccentricity of 0 Å. For the  $\text{Ac}^{3+}$  aqua ion its value is 0.14 Å, a small value bearing in mind that average Ac-O<sub>I</sub> distance is 2.66 Å. The coordination geometry is a second structural information associated to the symmetry which can be described by means of the OAcO angle distribution function (ADF) of the first shell obtained from



the MD simulation. Figure S5 in SI displays this function and compares it with the continuous ADFs which must be expected for ideal ennea-hydrate polyhedra with trigonal tri-capped prism (TTP) or gyro-elongated square anti-prism (Gy-SA) geometries. The  $\text{Ac}^{3+}$  aqua ion presents a geometry close to that of a GySA polyhedron as already shown in a previous work.<sup>19</sup> Both the high charge and the robustness of the aqua ion lead to a low translational diffusion coefficient,  $0.4 \cdot 10^{-5} \text{ cm}^2/\text{s}$  because it is the  $[\text{Ac}(\text{H}_2\text{O})_9]^{3+}$  the entity moving through the solution rather than the bare ion. Experimental and theoretical values for other octa- and ennea-hydrated trivalent cations are similar to the value found for  $\text{Ac}^{3+}$ .<sup>33,34</sup> A primary test of the energetic predictions of the employed interaction potentials is the  $\text{Ac}^{3+}$  hydration enthalpy computation at 300 K from the MD simulation. Our value,  $-708 \pm 13 \text{ kcal/mol}$ , underestimates slightly (2%-10%) the two experimental estimations.<sup>35,36</sup>

Table 2: Properties of  $\text{Ac}^{3+}$  aqueous solution.

Property	this work	Literature
$R_{\text{Ac-O}_\text{I}}$ (Å)	2.66	2.59, <sup>8</sup> 2.63-2.69, <sup>7</sup> 2.65 <sup>19</sup>
$\text{CN}_\text{I}$	8.9	9-10.9, <sup>7,9</sup> 9 <sup>19</sup>
DW (Å <sup>2</sup> )	0.014	
tilt angle <sub>I</sub> (°)	$28 \pm 15$	
$R_{\text{Ac-O}_\text{II}}$ (Å)	4.87	
$\text{CN}_\text{II}$	19.5	
tilt angle <sub>II</sub> (°)	$58 \pm 31$	
$\Delta\mu_\text{I}^{(\text{a})}$ (D)	$0.6 \pm 0.3$	
$\Delta\mu_\text{II}$ (D)	$0.1 \pm 0.3$	
MRT( $t^* = 0$ ) (ps)	$408 \pm 6$	
MRT( $t^* = 2$ ) (ps)	$623 \pm 18$	
$\Delta H_{\text{hyd}}$ (kcal/mol)	$-708 \pm 13$	$-725,$ <sup>36</sup> $-790$ <sup>35</sup>
$D$ ( $10^{-5} \text{ cm}^2/\text{s}$ )	$0.4 \pm 0.1$	

(a) Dipole moment change of water molecules with respect to the bulk value.

Figure 2 plots the experimental Ac L<sub>3</sub>-edge XANES spectrum (dotted line) of the  $\text{Ac}^{3+}$  aqueous solution measured by Ferrier et al.<sup>7</sup> at the SSRL. Two simulated XANES

spectra have been included in the same Figure. These simulated spectra are the average of 200 individual XANES spectra computed by means of the FEFF code (version 9.6),<sup>25</sup> taking evenly spaced snapshots from the 10 ns MD simulation. One of the simulated spectrum was built considering snapshots including the first hydration shell (red line), whereas the other simulated spectrum was built considering two hydration shells (blue line). FEFF input files have been included in SI. Because of the full multiple-scattering formalism employed in the ab initio computations, the absolute position of the computed edge is really close to the experimental one. The simulated 1-shell or 2-shell spectra were shifted  $-1.0$  and  $-2.0$  eV, respectively, in order to overimpose the experimental and theoretical white lines. It is remarkable the good reproduction of the experimental XANES, both in intensity and in position of the resonance above the white line, what according to Natoli's rule<sup>37</sup> implies that the Ac-O<sub>I</sub> distance provided by the MD simulation, i.e. the main contribution to the XAS spectrum, is consistent with the experimental XANES spectrum. An additional feature present in the experimental spectrum is the presence of a small hump 10 eV above the edge. We showed in previous studies<sup>20,21</sup> of stable aqua ions, such as those of Cr<sup>3+</sup>, Rh<sup>3+</sup> and Ir<sup>3+</sup>, that the appearance of this hump can be attributed to a well-defined second hydration shell. Likewise, for the case of Ni<sup>2+</sup> and Zn<sup>2+</sup> hydration, D'Angelo and col.<sup>38,39</sup> reached a similar conclusion. Allen et al. in a XAS study on lanthanoid and actinoid trivalent cations in LiCl and HCl aqueous solutions suggested that this XANES feature could be due to multiple scattering resonance appearing by changes in the inner sphere ligation.<sup>40</sup> Figure 2 (inset) shows how the simulated XANES spectrum built from the set of snapshots including the second hydration shell (blue line) shows that feature. Although the simulated spectrum is not able to fully reproduce the experimental slope changes, it clearly improves when the second shell is included in the calculation. This supports the structural information provided by the MD simulation and therefore the developed Ac<sup>3+</sup>-H<sub>2</sub>O interaction potential. An additional evidence on the origin of this XANES hump is related to the Ac L<sub>3</sub>-edge XANES spectrum measured by Ferrier et al.<sup>8</sup> for a highly concentrated (11 M) HCl aqueous solution. These authors

established from the EXAFS fitting that under these drastic conditions, the  $\text{Ac}^{3+}$  first coordination shell is formed by roughly three  $\text{Cl}^-$  and six  $\text{H}_2\text{O}$ . This multi-ligand and neutral  $\text{Ac}^{3+}$  complex cannot promote a well-defined second hydration shell and therefore no hump can be observed in its corresponding XANES spectrum (see top of Figure 2 of ref. [ 7]).

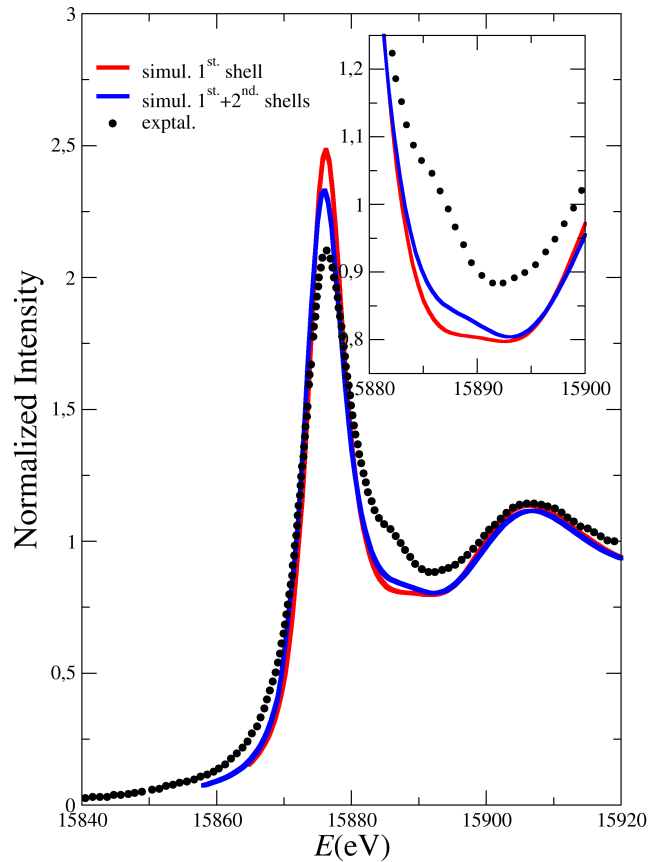


Figure 2: Comparison of the experimental (dotted lines)  $\text{Ac L}_3$  edge XANES spectrum of a very dilute  $\text{Ac}^{3+}$  aqueous solution<sup>7</sup> with the simulated one derived from MD structures using one or two hydration shells. Inset magnifies the region of the small hump.

The  $\text{Ac L}_3$   $k^3$ -weighted EXAFS spectrum of the  $\text{Ac}^{3+}$  in water has been computed by means of the average of 500 individual spectra using evenly-spaced snapshots taken from the MD trajectory. FEFF input files for the EXAFS computations have been included in SI. Figure 3 shows the comparison between the experimental spectrum<sup>7</sup> and the simulated

one, which includes the uncertainty calculated from the standard deviation associated to the average of 500 individual spectra. Figure S6 in SI shows the average simulated EXAFS spectrum of Figure 3 together with 10 randomly selected individual spectra taken from the set of spectra used for the average. The large difference among them clearly points out the need of a statistical average to obtain a meaningful result. Figure S7 in SI shows the comparison between the experimental and the average simulated Fourier Transform  $k^3$ -EXAFS spectra. There is a reasonable agreement of the average simulated spectrum with the experimental one, although some differences deserve to be analyzed. First of all, the intensity of the simulated signal is smaller than the experimental one, even if the uncertainty is considered. The high intensity of the experimental signal together with the use of a fixed DW factor of  $0.009 \text{ \AA}^2$  lead to an experimental fitted coordination number of 11.<sup>7</sup> The implicit DW factor for the Ac-O<sub>I</sub> distance of our simulation is computed from the second cumulant of  $R_{\text{Ac-O}_I}$  distribution ( $\sigma_{\text{Ac-O}_I}^2 = \langle R_{\text{Ac-O}_I}^2 \rangle - \langle R_{\text{Ac-O}_I} \rangle^2$ ). This value is  $0.015 \text{ \AA}^2$ , i.e. larger than the fixed value used in the experimental fitting. In addition, the average coordination number in the MD simulation is 9. As a consequence the overall EXAFS signal intensity of the simulated spectrum is a bit lower than the experimental one. The second source of discrepancy is a slight decoupling of the oscillation frequency. This can be easily visualized when examining the first three EXAFS oscillations in Figure 3 ( $2.5\text{-}6.7 \text{ \AA}^{-1}$  range). The simulated spectrum is a simple oscillation dominated by the contributions of the 2-leg Ac-O paths of the first shell: first-shell multiple scattering contributions and single scattering contributions due to second-shell Ac-O paths are residual.

These experimental-theoretical differences open the analysis of possible origins of the observed discrepancies. One of them could be that our structural description of the Ac<sup>3+</sup> aqueous solution is not refined enough to match the experimental behavior. The three basic parameters affecting the XAS spectrum are:  $R_{\text{Ac-O}_I}$ ,  $N_{\text{O}_I}$  and  $\sigma_{\text{Ac-O}_I}^2$ . The theoretical Ac-O distance must be correct according to the positions of the resonance above the white line in the XANES spectrum, following Natoli's rule,<sup>37</sup> and the oscilla-

tion frequency in the simulated EXAFS spectrum is also close to the experimental one. The second factor is the coordination number that our potential predicts to be nine, whereas experimental EXAFS fitting suggests eleven. QM computations for the decahydrate shows an increase of the Ac-O distance of  $\sim 0.04$  Å (see Table S4) compared to the ennea-hydrate value. The undecahydrated aqua ion structure cannot be optimized quantum-mechanically, but if this cluster was stable its distance would be  $\sim 0.03$  Å longer than in the decahydrate case. That hypothetical structure would have a mean  $R_{\text{Ac-O}_I}$  around  $0.07$  Å longer than the ennea-coordinated aqua ion, leading to an EXAFS frequency oscillation clearly higher than the experimentally observed one. In addition, a first shell formed by 11 H<sub>2</sub>O neither would it be able to promote a robust second hydration shell nor would it provide MS contributions inside the first shell to justify the slight non-simple oscillations observed in the experimental spectrum. At this point, we rather believe that the theoretical-experimental EXAFS spectrum difference must be joined to the high noise/signal ratio, and eventually to the presence of a small amount of another Ac<sup>3+</sup> complex formed in solution by the replacement of some water molecules by other ions present in the medium, such as triflate anion, lutetium or sodium cations.

The hump being present in the XANES spectrum which is ascribed to the second hydration shell and partially reproduced by the theoretical spectrum, suggests a relatively robust second hydration shell which would not be expected for a coordination number of 11. Figure S8 shows an example of the changes in the XANES spectrum of the optimized structures  $[\text{Ac}(\text{H}_2\text{O})_m]^{3+} (\text{H}_2\text{O})_n$ , for the combinations (m=8, n=16), (m=9, n=18) and (m=10, n=20). The corresponding one-shell  $[\text{Ac}(\text{H}_2\text{O})_m]^{3+}$  aqua ions (m=8, 9 and 10) ones are shown in Figure S9. It is shown how there is no hump in the case of the deca-hydrated aqua ion and how the energy difference between the white line and the first resonance becomes smaller as a consequence of the longer Ac-O<sub>I</sub> distance in the largest aqua ion (inset in Figure S8). Remarkably, all the XANES spectra of one-shell Ac<sup>3+</sup> clusters are hump-free as shown in Figure S9 of SI.

Several analysis based on structural QM computations and XAS simulations have

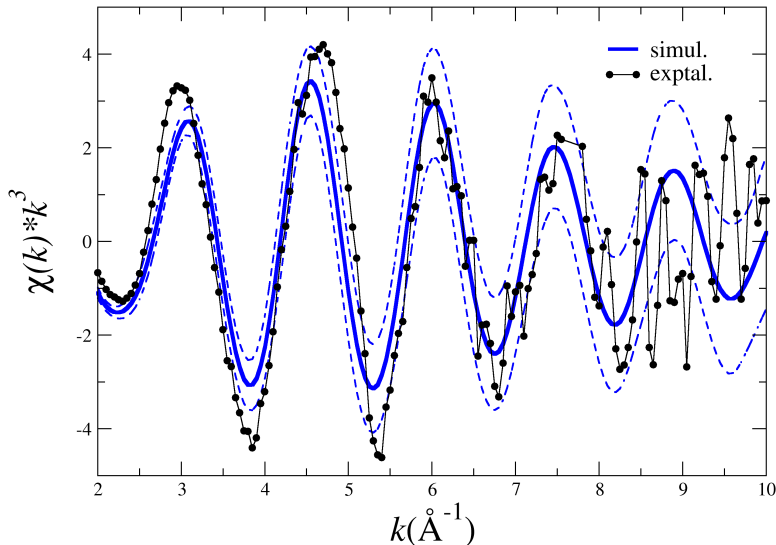


Figure 3: Comparison of the experimental (black dotted lines) Ac L<sub>3</sub>-edge  $k^3$ -weighted EXAFS spectrum of a very dilute Ac<sup>3+</sup> aqueous solution<sup>7</sup> with the simulated one from MD structures (blue line) with its statistical uncertainty (blue dashed lines).

shown the difficulties to conciliate the experimentally fitted coordination number of 11 with an average Ac-O<sub>I</sub> distance in the order of  $\sim 2.66$  Å. The extremely difficult experimental conditions needed to measure the Ac<sup>3+</sup> aqua ion lead to a rather noisy EXAFS spectrum what prevents an accurate fitting where there are not particular constraints between coordination number and distances. However, [Ac(H<sub>2</sub>O)<sub>m</sub>]<sup>3+</sup> QM computations contain intrinsically this constraint: an increase of the coordination number is associated to an Ac-O lengthening. Fortunately, XANES spectrum is less sensitive to the noise and combined with computer simulations helps to confirm, in an indirect way, the relationship between structural properties of the Ac<sup>3+</sup> environment in solution and spectroscopical features. Further studies including the description of aqueous solutions containing counterions, other electrolytes and different acid-base media, certainly will help in providing a wider analysis of the set of available experimental Ac<sup>3+</sup> samples.

## Conclusion

We have shown by computer simulations based on first-principles intermolecular potentials that the commendable experimental XAS spectra obtained by Ferrier et al.<sup>7</sup> are compatible with a coordination number of 9. This coordination number conciliates the behavior of the actinoid trivalent aqua ion series by ranging it between 9 and 8, as lanthanoid series, and providing in the case of the  $\text{Ac}^{3+}$  the longest An-O<sub>I</sub> distance,  $2.66\pm 0.02$  Å. This result supports the smooth actinoid contraction of aqua ions along the series. The structural and dynamical properties of the  $\text{Ac}^{3+}$  hydrate shows that it is a good example of a robust aquaion with a well defined second hydration shell and a long residence time of water molecules in its first hydration shell.

## Acknowledgement

We would like to dedicate this work to Prof. Jean-Paul Malrieu, University of Toulouse on the occasion of his 80<sup>th</sup> birthday. This work was financially supported Junta de Andalucía of Spain (FQM-282). DZC thanks to Junta de Andalucia of a postdoctoral fellowship. We thank Dr. Kozimor for supplying us with the experimental EXAFS and XANES spectra of the  $\text{Ac}^{3+}$  aqueous solution.

## Supporting Information Available

Representative structures employed in the potential development; text detailing functional forms of the MCDHOs potential and Ac-H<sub>2</sub>O fitted parameters; plot of QM vs. potential interaction energy of the set of structures used for the fit, table of geometries of several  $[\text{Ac}(\text{H}_2\text{O})_m]^{3+}(\text{H}_2\text{O})_n$  clusters; plots of  $\text{Ac}^{3+}$  clusters containing 10 water molecules: (8+2),(9+1) and (10) where second-shell water molecules only form one hydrogen bond with first-shell water molecules; OAcO angle distribution function for  $\text{Ac}^{3+}$  in water simulation and comparison with continuous ADFs of ideal polyhedra with GySA

and TTP geometries; simulated EXAFS spectra of a set of individual snapshots, and average spectrum of the simulation; experimental vs. simulated Fourier Transform  $k^3$ -EXAFS spectra; comparison of experimental vs simulated XANES spectra for a set of  $\text{Ac}^{3+}$  hydrated clusters with one or two hydration shells, FEFF input files for EXAFS and XANES calculations.

## References

- (1) Choppin, G. R.; Jensen, M. P. In *The Chemistry of the Actinide and Transactinide Elements*, 3rd ed.; Morss, L. R., Edelstein, N., Fuger, J., Katz, J. J., Eds.; Springer, 2008; Vol. 4; Chapter 23, pp 2524–2621.
- (2) Altmaier, M.; Gaona, X.; Fanghänel, T. Recent Advances in Aqueous Actinide Chemistry and Thermodynamics. *Chem. Rev.* **2013**, *113*, 901–943.
- (3) Denecke, M. A. Actinide speciation using X-ray absorption fine structure spectroscopy. *Coord. Chem. Rev.* **2006**, *250*, 730–754.
- (4) Evrarda, O.; Lacebya, J. P.; Lepagea, H.; Ondab, Y.; Cerdanc, O.; Ayrault, S. Radiocesium Transfer from Hillslopes to the Pacific Ocean after the Fukushima Nuclear Power Plant Accident: A Review. *J. Environm. Rad.* **2015**, *148*, 92–110.
- (5) Ulmert, D.; Abou, D.; Lilja, H.; Larson, S.; Thorek, D. Targeted Alpha-particle Therapy of Disseminated Prostate Cancer with  $^{225}\text{Ac}$ . *J. Nucl. Med.* **2015**, *56* (suppl.3), 281.
- (6) Albrecht-Schmitt, T. Fleeting Glimpse of an Elusive Element. *Nature* **2016**, *536*, 404–405.
- (7) Ferrier, M. G.; Stein, B. W.; Batista, E.; Berg, J.; Birnbaum, E. R.; Engle, J. W.; John, K. D.; Kozimor, S. A.; Lezama Pacheco, J. S.; Redman, L. N. Synthesis and Characterization of the Actinium Aquo Ion. *ACS Cent. Sci.* **2017**, *3*, 176–185.



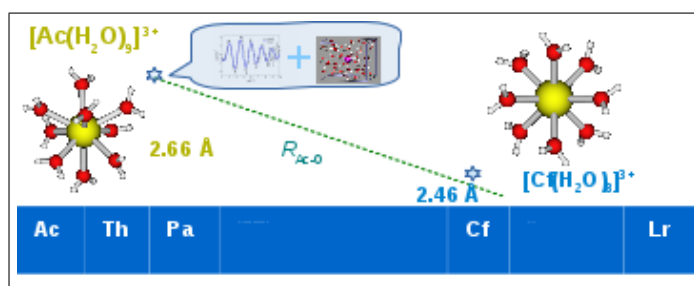
- (8) Ferrier, M. G.; Batista, E.; Berg, J.; Birnbaum, E. R.; Cross, J. N.; Engle, J. W.; La Pierre, H. S.; Kozimor, S. A.; Lezama Pacheco, J. S.; Stein, B. W.; Stieber, S. C. E.; Wilson, J. Spectroscopic and Computational Investigation of Actinium Coordination Chemistry. *Nat. Commun.* **2016**, *7*, 12312(1)–(8).
- (9) Ferrier, M. G.; Stein, B. W.; Bone, S. E.; Cary, S. K.; Ditter, A. S.; Kozimor, S. A.; Lezama Pacheco, J. S.; Mocko, V.; Seidler, G. T. The Coordination Chemistry of Cm<sup>III</sup>, Am<sup>III</sup>, and Ac<sup>III</sup> in nitrate solutions. an actinide L<sub>3</sub>-edge EXAFS study. *Chem. Sci.* **2018**, *9*, 7078–7090.
- (10) Persson, I.; D’Angelo, P.; De Panfilis, S.; Sandström, M.; Eriksson, L. Hydration of Lanthanoid(III) Ions in Aqueous Solution and Crystalline Hydrates Studied by EXAFS Spectroscopy and Crystallography: The Myth of the “Gadolinium Break”. *Chem. Eur. J.* **2008**, *14*, 3056–3066.
- (11) Apostolidis, C.; Schimmelpfennig, B.; Magnani, N.; Lindqvist-Reis, P.; Walter, O.; Sykora, R.; Morgenstern, A.; Colineau, E.; Caciuffo, R.; Klenze, R.; Haire, R.; Rebizant, J.; Bruchertseifer, F.; Fanghänel, T. [An(H<sub>2</sub>O)<sub>9</sub>](CF<sub>3</sub>SO<sub>3</sub>)<sub>3</sub> (An = U–Cm, Cf): Exploring Their Stability, Structural Chemistry, and Magnetic Behavior by Experiment and Theory. *Angew. Chem. Int. Ed.* **2010**, *49*, 6343–6347.
- (12) D’Angelo, P.; Martelli, F.; Spezia, R.; Filipponi, A.; Denecke, M. Hydration Properties and Ionic Radii of Actinide(III) Ions in Aqueous Solution. *Inorg. Chem.* **2013**, *52*, 10318–10324.
- (13) Spezia, R.; Migliorati, V.; D’Angelo, P. On the development of polarizable and Lennard-Jones force fields to study hydration structure and dynamics of actinide(III) ions based on effective ionic radii. *J. Chem. Phys.* **2017**, *147*, 161707(1)–(11).
- (14) Lundberg, D.; Persson, I. The Size of Actinoid(III) Ions - Structural Analysis vs. Common Misinterpretations. *Coord. Chem. Rev.* **2016**, *318*, 131–134.

- (15) Martínez, J. M.; Pappalardo, R. R.; Sánchez Marcos, E. First-Principles Ion-Water Interaction Potentials for Highly Charged Monoatomic Cations. Computer Simulations of  $\text{Al}^{3+}$ ,  $\text{Mg}^{2+}$  and  $\text{Be}^{2+}$ . *J. Am. Chem. Soc.* **1999**, *121*, 3175–3184.
- (16) Galbis, E.; Hernández-Cobos, J.; den Auwer, C.; Le Naour, C.; Guillaumont, D.; Simoni, E.; Pappalardo, R. R.; Sánchez Marcos, E. Solving the Hydration Structure of the Heaviest Actinide Aqua Ion Known: The Californium (III) Case. *Angew. Chem. Int. Ed.* **2010**, *122*, 3899–3903.
- (17) Galbis, E.; Hernández-Cobos, J.; Pappalardo, R.; Sanchez Marcos, E. Collecting High-order Interactions in an Effective Pairwise Intermolecular Potential Using the Hydrated Ion Concept: The Hydration of Cf(III). *J. Chem. Phys.* **2014**, *140*, 214104–(1)–(11).
- (18) Caralampio, D. Z.; Martínez, J. M.; Pappalardo, R. R.; Sánchez Marcos, E. Development of a polarizable and flexible model of the hydrated ion potential to study the intriguing case of Sc(III) hydration. *Theor. Chem. Acc.* **2017**, *136*, 47(1–8).
- (19) Morales, N.; Galbis, E.; Martínez, J. M.; Pappalardo, R. R.; Sánchez Marcos, E. Identifying Coordination Geometries of Metal Aqua Ions in Water: Application to the Case of Lanthanoid and Actinoid Hydrates. *J. Phys. Chem. Lett.* **2016**, *7*, 4275–4280.
- (20) Merklings, P. J.; Muñoz-Páez, A.; Sánchez Marcos, E. Exploring the Capabilities of X-Ray Absorption Spectroscopy for Determining the Structure of Electrolyte Solutions: Computed Spectra for  $\text{Cr}^{3+}$  or  $\text{Rh}^{3+}$  in Water Based on Molecular Dynamics. *J. Am. Chem. Soc.* **2002**, *124*, 10911–10920.
- (21) Carrera, F.; Torrico, F.; Richens, D. T.; Muñoz-Páez, A.; Martínez, J. M.; Pappalardo, R. R.; Sánchez Marcos, E. Combined Experimental and Theoretical Approach to the Study of Structure and Dynamics of the Most Inert Aqua Ion  $[\text{Ir}(\text{H}_2\text{O})_6]^{3+}$  in Aqueous Solution. *J. Phys. Chem. B* **2007**, *111*, 8223–8233.

- (22) Pérez-Conesa, S.; Martínez, J. M.; Pappalardo, R. R.; Sánchez Marcos, E. Extracting the Americyl Hydration from an Americium Cationic Mixture in Solution: A Combined X-ray Absorption Spectroscopy and Molecular Dynamics Study. *Inorg. Chem.* **2018**, *57*, 8089–8097.
- (23) Rehr, J. J.; Albers, R. Theoretical Approaches to X-Ray Absorption Fine Structure. *Rev. Mod. Phys.* **2000**, *72*, 621–654.
- (24) Ankudinov, A. L.; Nesvizhskii, A. I.; Rehr, J. J. Dynamic Screening Effects in X-Ray Absorption Spectra. *Phys. Rev. B* **2003**, *67*, 115120.
- (25) Rehr, J. J.; Kas, J. J.; Vila, F. D.; Prange, M. P.; Jorissen, K. Parameter-free calculations of x-ray spectra with FEFF9. *Phys. Chem. Chem. Phys.* **2010**, *12*, 5503–5513.
- (26) Saint-Martin, H.; Hernández-Cobos, J.; Bernal-Uruchurtu, M. I.; Ortega-Blake, I.; Berendsen, H. J. C. A mobile charge densities in harmonic oscillators (MCDHO) molecular model for numerical simulations: The water-water interaction. *J. Chem. Phys.* **2000**, *113*, 10899–10912.
- (27) Villa, A.; Hess, B.; Saint-Martin, H. Dynamics and structure of Ln(III) Aqua Ions: A Comparative Molecular Dynamics study using ab Initio based flexible and polarizable model potentials. *J. Phys. Chem. B* **2009**, *113*, 7270–7281.
- (28) Staroverov, V. N.; Scuseria, G.; Tao, J.; Perdew, J. Comparative assessment of a new nonempirical density functional: Molecules and hydrogen-bonded complexes. *J. Chem. Phys.* **2013**, *119*, 12129–12137.
- (29) Frisch, M. J. et al. Gaussian 09 Revision D.01. 2009; Gaussian Inc. Wallingford CT.
- (30) Todorov, I. T.; Smith, W.; Trachenko, K.; Dove, M. T. DL\_POLY\_3: New Dimensions in Molecular Dynamics Simulations Via Massive Parallelism. *J. Mat. Chem.* **2006**, *16*, 1911–1918.

- (31) Impey, R.; Madden, P.; McDonald, I. Hydration and mobility of ions in solution. *J. Phys. Chem.* **1983**, *87*, 5071–5083.
- (32) Caralampio, D. Z.; Martínez, J. M.; Pappalardo, R. R.; Sánchez Marcos, E. The hydration structure of the heavy-alkalines Rb<sup>+</sup> and Cs<sup>+</sup> through molecular dynamics and X-ray absorption spectroscopy: surface clusters and eccentricity. *Phys. Chem. Chem. Phys.* **2017**, *19*, 28993–29004.
- (33) Richens, D. T. *The Chemistry of Aqua Ions*; John Wiley: Chichester, 1997.
- (34) Marcus, Y. *Ions in Solution and Their Solvation*; John Wiley & Sons, 2015.
- (35) Marcus, Y. The Thermodynamics of Solvation of Ions.2. The Enthalpy of Hydration at 298.15-K. *J. Chem. Soc. Faraday Trans. 1* **1987**, *83*, 339–349.
- (36) Abramov, A. A.; Eliseeva, O. V.; Iofa, B. Z. Prediction of physicochemical constants of francium, radium, and actinium. *Radiochemistry* **1998**, *40*, 302–305.
- (37) Bianconi, A.; Dell’Ariccia, M.; Gargano, A.; Natoli, C. R. In *Springer Series in Chemical Physics*; Bianconi, A., Incoccia, A., Stipcich, S., Eds.; Springer, 1983; Vol. 27; pp 57–61.
- (38) D’Angelo, P.; Roscioni, O. M.; Chillemi, G.; Della Longa, S.; Benfatto, M. Detection of Second Hydration Shells in Ionic Solutions by XANES: Computed Spectra for Ni<sup>2+</sup> in Water Based on Molecular Dynamics. *J. Am. Chem. Soc.* **2006**, *128*, 1853–1858.
- (39) Migliorati, V.; Zitolo, A.; Chillemi, G.; D’Angelo, P. Influence of the Second Coordination Shell on the XANES Spectra of the Zn<sup>2+</sup> Ion in Water and Methanol. *ChemPlusChem* **2012**, *77*, 234–239.
- (40) Allen, P.; Bucher, J. J.; Shuh, D. K.; Edelstein, N. M.; Craig, I. Coordination Chemistry of Trivalent Lanthanide and Actinide Ions in Dilute and Concentrated Chloride Solutions. *Inorg. Chem.* **2000**, *39*, 595–601.

## Graphical TOC Entry



Structural determination of the lightest Actinoid aqua ion,  $[\text{Ac}(\text{H}_2\text{O})_9]^{3+}$  supports the actinoid contraction along the series.  $2.66 \text{ \AA}$  is the Ac-O distance in the first shell.